In: Robotics, Computer Vision and Intelligent Systems. ROBOVIS 2020 2021.
Communications in Computer and Information Science, vol 1667, pp. 114-130
DOI: 10.1007/978-3-031-19650-8_6

Visual guidance of an on-orbit free-floating manipulator using a mobile camera

José L. Ramón[1[0000-0002-8635-6061]], Jorge Pomares[1[0000-0002-7523-9118]], and Leonard Felicetti[2[0000-0001-6830-4308]]

[1] University of Alicante, Alicante, 03690, Spain
jl.ramon@ua.es, jpomares@ua.es
[2] Cranfield University, Cranfield, MK43 0AL, United Kingdom
Leonard.Felicetti@cranfield.ac.uk

Abstract. A direct visual-servoing algorithm for control a space-based manipulator is proposed. A two-arm manipulator is assumed as a baseline scenario for this investigation, with one of the arms performing the manipulation and the second arm dedicated to the observation of the target zone of manipulation. The algorithm relies on images taken independently from de-localized cameras, e.g. at the end-effector of a second manipulator. Through the implementation of a Kalman filter, the algorithm can estimate the movements of the features in the image plane due to the relative movements between the camera and the target and then calculate the torques to be provided to the joints of the manipulator by adopting a visual servoing control strategy. Simulations results in two different scenarios have been presented to show an adequate behaviour of the presented approach in on-orbit-servicing operations.

Keywords: Space Robotics, On-Orbit Servicing, Visual Servoing, Impedance Control.

1 Introduction

We are now entering a new and exciting phase that is changing the paradigms of exploitation of near-Earth space and its resources. In the sixties and seventies, space activities were carried on primarily for governmental or military purposes, intended more to assert the technical and strategical supremacy of one nation over the others. From the eighties up to the end of the twentieth century, the need for word-wide services led to the raise of telecommunications and commercial players into the space race scene. The race for space exploitation is now changing again, with private actors developing a whole new series of activities and economic business opportunities [1]. The change is exponentially growing due to a sensible increase of the number of launch opportunities, the reduction of the overall missions' costs and numerous investments for making space the new domain for carrying on and supporting word-wide commercial and economic activities. This necessarily is leading to an exponential growth of the objects populating near-Earth regions. According to the United Nations Office for Outer Space Affairs [2], only in 2021 more than 1700 objects were

Published by Springer. This is the Author Accepted Manuscript.
The final published version (version of record) is available online at DOI:10.1007/978-3-031-19650-8_6. Please refer to any applicable publisher terms of use.

launched into space. Initially, most of the failures occurred during launch and early operations phases, but nowadays, many more failures occur once the satellites are operating in orbit. Even if no failures occur, the mission's lifetime is limited by the amount of fuel and other consumable items carried onboard by spacecraft. For example, in some applications, once the fuel necessary to perform station keeping and attitude maneuvers is finished, the satellite is forced to finish its mission and be dismissed, even if all the other systems would be able to continue to carry on their nominal activities for longer time. Recent studies show that repairing or refuelling these satellites would reduce costs significantly [3].

For this reason, agencies are interested in the field of in-orbit servicing. Another aspect to consider is that a large quantity of such newly inserted in orbit objects is destined to increase space debris population. Thus, numerous current research activities and under development missions are exploring and assessing the feasibility of active debris removal strategies [4].

Some of the mission concepts for on-orbit servicing and active debris removal utilize robotic manipulators for performing complex operations, such as grasping, manipulation, refuelling, inspections and many others. Space environmental conditions, such as free-floating and frictionless conditions, impose new challenges for the control of such robotic systems: classical strategies for Earth-based manipulators are generally not applicable to space-based manipulators. In addition, most of the foreseen on-orbit operations in future missions impose strict requirements in terms of precision and accuracy of the robotic arm movements, and in some cases, these operations will need to be performed with a high level of autonomy. Most of the missions carried out in the last two decades had robotic operations mainly under teleoperation or manual control (e.g. robotic arms in the International Space Station). Teleoperation of space robotic assets are currently limited by the eventual delays in communications and strict requirements necessary to maintain constant communication between the robotic manipulator and the operators. These issues become even more critical when the spacecraft operates far from Earth (i.e., in deep space and planetary exploration missions). This way of using on-orbit robotic systems is destined to disappear in favour of more autonomous systems that will decide and carry-on operations based on in-situ measurements and evaluation of the necessary operations to be performed without any human-in-the-loop.

Robotic on-orbit service (OOS) and active debris removal (ADR) missions are generally composed of three elements. The servicing spacecraft, a robotic manipulator, attached to the service spacecraft and, finally, the target spacecraft to be served. In active debris removal missions, the target spacecraft is replaced by the space debris element that needs to be removed from a certain orbital position. One of the challenges in OOS and ADR missions is represented by the uncooperativeness of the target objects, either because they have reached the end of their useful life or because they have faulty or uncontrolled parts [5]. These missions are also characterized by a set of standard phases that span from the launch and early operations when the servicing spacecraft is inserted in orbit, orbital manoeuvres to reach the target's orbit, a rephasing and approach phase that allows for having the service spacecraft in close proximity to the target, a synchronization phase that enables to minimize the relative velocity

with respect target's motion, the rendezvous and docking/grasping phase and the subsequent phase where all the robotic operations are performed as well as the disengagement operations that terminates the specific operations to a specific target [6].
This paper focuses on the control strategies for driving the robotic manipulator once the approach and synchronization phases have been already accomplished by the service spacecraft and the final rendezvous/grasping phase needs to be performed. Having a reliable and robust control becomes of vital importance in such a phase, as it is extremely important to avoid unintentional collisions that could cause damage or determine the mission failure [7].
The relative position between the spacecraft and the target must be continuously monitored to avoid collisions [8]. Among the possible means to know the relative position between spacecraft, we have opted for using cameras as a sensor because of their reliability and versatility than other types of sensors [8]. There are three main options for the location of the camera system within the service spacecraft. The first option considers a fixed camera installed on the main spacecraft's body in a favourable position to oversee the operations and movements performed by the robotic manipulator. The second possible option uses an eye-in-hand configuration, where the camera is placed at the manipulator's end effector. The third and final option uses a camera installed on an auxiliary mobile reconfigurable structure. The latter is the option that we consider in this work. The problem presented by the first option is the risk of occlusions produced by the manipulator itself, preventing the realization of visual control. The second option improves this aspect since the camera moves together with the robot's end-effector but does not eliminate the possibility of occlusions in specific configurations. The adopted option offers a higher degree of versatility with the possibility of moving the camera constantly to have the best possible view that allows for each operation in any task performed by the robotic arm [9][10]. This article focuses on the specific scenario where the service spacecraft is equipped with two robotic arms. The first of the arms will be in charge of performing the manipulation tasks, while the second one carries on a camera at its end-effector that moves to guarantee an optimal observation of the robotic operations and avoids eventual occlusions of the observed scene [11].
The paper proposes a new approach where both the service spacecraft and the target are in free-floating conditions at a sufficient distance so that the manipulator is able to perform its grasping and manipulation operations [12]. The visual servoing controller part is a well-known controller [15] for manipulator control using information obtained from cameras. In this type of control, it is not necessary to perform a 3D reconstruction of the target position to guide the robot since it only uses information extracted from the images captured by the camera. The proposed controller obtains the error directly from the image plane, directly giving torques to be applied in each of the manipulator's joints as a result. In this way, it is not necessary to either estimate the relative pose of the target with respect to the servicing spacecraft as well as to solve any complex inversion of the kinematic and dynamics of the manipulators for obtaining torques to be provided by servomotors. This last feature offers advantages, especially for the guidance of free-floating space robots, with eventual actions on the main body of the service spacecraft directly calculated by the controller itself, as al-

ready done by the authors in [13]. Visual servoing is also applied for the control of free-floating robots based directly on images, with an eye-in-hand configuration in [16] or, as done in [17], for the guidance of a spacecraft during a rendezvous manoeuvre. In this paper, the scenario proposed in [11] is considered where a camera installed at the end of the second manipulator is used to observe the target features. These features are used by the controller to calculate the control actions independently of the camera position. However, the present study focuses on the estimation problem of the eventual trajectories of the visual features, which might move due to both the motion of the manipulators of the servicing spacecraft as well as the motion of the target. The proposed approach uses Kalman filter as a tool for the estimation of the movements of the visual features in the image plane. Such estimations can be included within the visual servoing controller to obtain a robust and reliable tool that allows for moving and catching targets that are also moving with respect to the servicing spacecraft. This paper explores such an approach and provides simulations for demonstrating the viability of the methodology.
The rest of the article is organized as follows. Section 2 presents a description of the scenario, including the architecture of the service spacecraft and the key characteristics of the manipulators installed on it. Section 3 describes the visual servo control of the manipulator in detail, focusing on the estimation of the movements of the visual features and of the target motion via a Kalman filter implementation. Such estimations will then be used within ad-hoc build visual servoing controllers that track specific trajectories in the image in the specific free-floating base case. This is described in Section 4 with a resulting control law that will be then used to drive the robotic manipulator in test case simulation scenarios. The results obtained from the simulations are presented in Section 5. Finally, Section 6 summarize the main findings obtained in the present investigation.

2 Robotic spacecraft

This section presents the main details of the robotic spacecraft and the on-orbit servicing scenario considered in this paper. A servicing spacecraft is equipped with two robotic arms: the main dynamic parameters of the servicing spacecraft and the robotic arms are indicated in Table 1 and Table 2, respectively (both robotic arms have the same dynamic parameters). One of the robotic arms (robotic camera) presents a camera at its end-effector and extracts the visual features from a target spacecraft to perform the guidance of the other robotic arm (robotic manipulator). Image extraction and processing are not addressed in this paper, and it is supposed that these can be performed so that the controller can get and track a pattern with m points of the target spacecraft.

Figure 1 represents the on-orbit servicing scenario considered in this paper. As previously indicated, a set of m visual features are extracted from the target using the robotic camera, C. With B is represented the coordinate frame at the servicing spacecraft centre of mass, and E represents the coordinate frame at the end of the manipulator robot. Finally, an earth-centred inertial coordinate frame, called I is used.

Table 1. Dynamic parameters of the servicing spacecraft.

Mass (Kg)	Inertia(kg·m^2)		
	I_x	I_y	I_z
2550	6200	3550	7100

Table 2. Dynamic parameters of the servicing spacecraft.

		Inertia		
Arms	Mass (Kg)	I_x	I_y	I_z
Link1	35	2	0.2	2
Link2	22	3	0.2	3
Link3	22	3	0.2	3
Link4	12	0.1	0.2	0.4
Link5	12	0.1	0.2	0.3
Link6	10	0.2	0.25	0.3

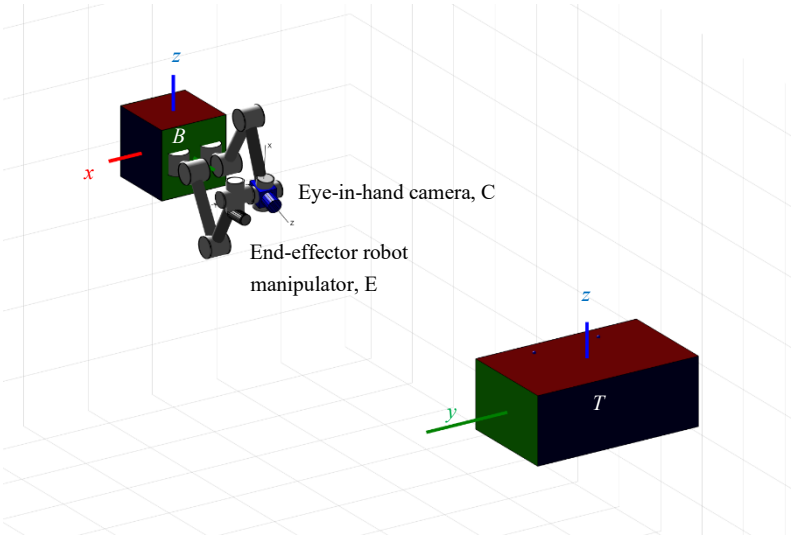

Fig. 1. Servicing spacecraft and extracted visual features.

3 Visual servoing of a manipulator and estimation of the target motion in the image space

An image-based visual servoing system directly uses visual features extracted from the images obtained by the camera to generate control actions of the manipulator to track and converge progressively toward the desired features in the image plane. This approach differs from position-based controllers in that it is not necessary to calculate the 3-D pose of the observed object. This way, the control is performed directly in the image space. This paper assumes that the image processing algorithms can always extract specific points as visual features of the target. This set of points is represented with the variable $\boldsymbol{s}$. The visual controller must apply the control actions in such a way that set $\boldsymbol{s}$ progresively reaches the value of the desired features, $\boldsymbol{s}_d$. In this way, an error function is defined, and the objective of the controller is to reduce the value of such an error function progressively. In the next paragraphs, classical visual servoing systems are modified to allow the manipulator guidance when the visual features are obtained from a mobile camera (the robotic camera in this paper). Additionally, the estimation of the target motion is included in the next section to improve the controller behaviour during the tracking.

3.1 Visual controller using the robotic camera

In the previous paragraphs, the main properties of the employed image-based controller are described. However, in order to guide the manipulator robot, some modifications must be performed in the previous approach. The classical image-based controller considers that an eye-in-hand camera is employed. However, the camera is located at the end of the robotic camera in our case. To overcome this problem, a virtual camera located at the end of the manipulator robot is considered. This virtual camera will be employed to simulate the use of an eye-in-hand camera at the manipulator robot. This controller presents several improvements with respect the one described in our previous work [11]. The presented approach allows to determine the 3D pose of the target spacecraft frame with respect to the robotic camera only using image information. Additionally, the pose of the characteristic points with respect to the virtual camera can be obtained. Finally, this last information is projected in the image space to obtain the visual features employed by the visual servoing system. Therefore, the visual servoing can be performed independently on the point of view. These steps will be described in the next paragraphs.

First, we consider $\boldsymbol{M}_T^C$ as extrinsic parameters of the real camera located at the end of the robotic camera (pose of the target spacecraft frame with respect to the robotic camera frame). A target 3D point, $\boldsymbol{P}_{Pi}^T$, can be expressed in the robotic camera coordinate frame as:

$$\boldsymbol{P}_{Pi}^C(x_P^C, y_P^C, z_P^C) = \boldsymbol{M}_T^C \boldsymbol{P}_{Pi}^T \tag{1}$$

Considering a pin-hole camera projection model, the point $\boldsymbol{P}_P^C$, expressed with respect to the camera reference frame, is projected onto the image plane at the 2D point $\boldsymbol{p}_i$. This point is computed from the camera focal length, f, as:

$$\boldsymbol{p}_i = (x_i, y_i)^T = \left(f\frac{x_{Pi}^C}{z_{Pi}^C}, f\frac{y_{Pi}^C}{z_{Pi}^C} \right)^T \tag{2}$$

Finally, the units of (2) specified in terms of metric units are scaled and transformed in pixels coordinates relative to the image reference frame, as:

$$\boldsymbol{s}_i = \left(f_{ix}, f_{iy}\right)^T = (u_0 + f_u x_i, v_0 + f_v y_i)^T \tag{3}$$

where $\boldsymbol{s}_i = \boldsymbol{s}_i\big(\boldsymbol{r}(t)\big)$, and $\boldsymbol{r}(t)$ is the relative pose between the camera and inertia frame and (f_u, f_v, u_0, v_0) are the camera intrinsic parameters. The intrinsic parameters considered are the position of the optical center (u_0, v_0), and ($f_u = s_x$, $f_v = s_y$) represent the focal length in terms of pixels, where s_x and s_y are the scale factors relating pixels to distance.

In order to perform the manipulator robot guidance using the virtual camera, the following steps have been implemented:

1. First, $\boldsymbol{s} = (\boldsymbol{s}_1, \boldsymbol{s}_2, \cdots, \boldsymbol{s}_m)^T$ is considered as the extracted visual features by the robotic camera. From these visual features, the pose of the target spacecraft frame with respect to the robotic camera, $\boldsymbol{M}_T^C$ must be obtained (estimation of the camera extrinsic parameters). The estimation of these extrinsic parameters will be done by the definition of the following error function:

$$\boldsymbol{e} = \boldsymbol{s}_v - \boldsymbol{s} \tag{4}$$

Where $\boldsymbol{s}$ have been defined as the extracted visual features and $\boldsymbol{s}_v$ is the image position of the same features computed by back-projection employing the estimated extrinsic parameters. Therefore, it is required to define a control function that reduces the previous error function by modifying the extrinsic parameters. Please note that when this error function is zeroed, the estimated extrinsic parameters will be the real ones of the camera. To enable this, the time derivative of the error function is computed as:

$$\dot{\boldsymbol{e}} = \dot{\boldsymbol{s}}_v - \dot{\boldsymbol{s}} = \frac{\partial \boldsymbol{s}_v}{\partial \boldsymbol{r}}\frac{\partial \boldsymbol{r}}{\partial t} = \boldsymbol{L}_s \frac{\partial \boldsymbol{r}}{\partial t} \tag{5}$$

where $\boldsymbol{L}_s$ is the interaction matrix used in classical image-based visual servoing systems [15]. A proportional control law is defined to reduce the error function. Specifically, an exponential decrease of the error, $\boldsymbol{e}$, is imposed by $\dot{\boldsymbol{e}} = -\lambda_1 \boldsymbol{e}$, being λ_1 a positive gain. Therefore, the following control action is obtained:

$$\frac{\partial \boldsymbol{r}}{\partial t} = -\lambda_1 \boldsymbol{L}_s^+ \boldsymbol{e} \tag{6}$$

2. Using the previous step, the pose of the target spacecraft frame with respect to the robotic camera is obtained $\boldsymbol{M}_T^C$. From the spacecraft kinematics, it is also possible to obtain the relative position between the robotic camera and the virtual camera located at the end of the manipulator robot, $\boldsymbol{M}_C^{VC}$. The homogeneous transformation matrix between the target spacecraft T and the virtual camera, VC, can easily be obtained as $\boldsymbol{M}_T^{VC} = \boldsymbol{M}_C^{VC}\boldsymbol{M}_T^C$.
3. A kinematic model of the features extracted from the target spacecraft is known so the 3D position of each of the characteristic points with respect the frame T is known, $\boldsymbol{P}_i^T$. Using this information and the matrix $\boldsymbol{M}_T^{VC}$, the pose of the characteristic points with respect to the virtual camera is equal to $\boldsymbol{P}_i^{VC} = \boldsymbol{M}_T^{VC}\boldsymbol{P}_i^T$. Considering $(x_i^{VC}, y_i^{VC}, z_i^{VC})$ the coordinates of the previous pose, Equations (2) and (3) can be used to obtain the value of the visual features in pixel coordinates in the image space, $\boldsymbol{s}_i$. These features will be the extracted features at each iteration of the task.
4. In order to guide the manipulator robot, an image-based visual servoing system can be applied. This approach allows the tracking of a given trajectory by using visual information. This control action can be performed from the visual features $\boldsymbol{s}_i$ and the desired positions of these features $\boldsymbol{s}_{id}$, i. e., the value of these features in the desired location to be achieved. From the previous features, it is possible to define the set of observed and desired visual features as $\boldsymbol{s} = (\boldsymbol{s}_1, \boldsymbol{s}_2, \cdots, \boldsymbol{s}_m)^T$ and $\boldsymbol{s}_d = (\boldsymbol{s}_{1d}, \boldsymbol{s}_{2d}, \cdots, \boldsymbol{s}_{md})^T$ respectively, and the control action as:

$$\boldsymbol{v}^{VC} = -\lambda_2 \boldsymbol{L}_s^{+}(\boldsymbol{s} - \boldsymbol{s}_d) \tag{7}$$

where $\boldsymbol{v}^{VC}$ are the velocities to be applied with respect to the virtual camera and λ_2 a positive control gain.

3.2 Estimation of the target spacecraft motion in the image space

The visual servoing system presented in the previous section does not take into account the eventual movements of the target satellite. This section extends the previous visual servoing system to include the estimation of the target spacecraft's motion and better track the trajectories in the image space when the target is in motion. To do this, it is necessary to estimate the variations in the image error due to the motion of the target spacecraft and include it in the computation of the control actions.

The expression that relates the control action with respect to the virtual camera coordinate frame, the image error and the image error estimation due to the motion of the target spacecraft is:

$$\boldsymbol{v}^{VC} = \left(\frac{\partial \widehat{\boldsymbol{e}_s}}{\partial \boldsymbol{r}}\right)^{+} \left(-\lambda \boldsymbol{e}_s - \frac{\partial \widehat{\boldsymbol{e}_s}}{\partial t}\right) \tag{8}$$

where $\boldsymbol{e}_s = \boldsymbol{s} - \boldsymbol{s}_d$ is the image error that needs to be minimized. The estimation of the motion velocity of the target spacecraft using an eye-in-hand camera system can be obtained from the camera velocities measurements and the error function. Therefore, from Equation (8) we can obtain the value of the estimation of the error variation due to the motion of the target spacecraft (note that the proportional control action

allows for obtaining an exponential decrease of the error function and, therefore, $\dot{\boldsymbol{e}}_s = -\lambda \boldsymbol{e}_s$):

$$\frac{\partial \widehat{\boldsymbol{e}_s}}{\partial \boldsymbol{r}} = \dot{\boldsymbol{e}}_s - \frac{\partial \widehat{\boldsymbol{e}_s}}{\partial t} \boldsymbol{v}^{VC} \tag{9}$$

To obtain the value of the estimation of the motion at each iteration, a discretization of Equation (9) can be done, obtaining the following expression:

$$\left(\frac{\partial \widehat{\boldsymbol{e}_s}}{\partial t}\right)_k = \frac{\boldsymbol{e}_k - \boldsymbol{e}_{k-1}}{\Delta t} - \frac{\partial \widehat{\boldsymbol{e}_s}}{\partial \boldsymbol{r}} \boldsymbol{v}^{VC} \tag{10}$$

where Δt can be obtained by computing the delay at each iteration. Additionally, the term $\frac{\partial \widehat{\boldsymbol{e}_s}}{\partial r}$ is equal to the identity matrix, and therefore (10) can be simplified in the following relationship:

$$\left(\frac{\partial \widehat{\boldsymbol{e}_s}}{\partial t}\right)_k = \frac{\boldsymbol{e}_k - \boldsymbol{e}_{k-1}}{\Delta t} - \boldsymbol{v}^{VC} \tag{11}$$

Therefore, Equation (11) can be used to measure the image error variation due to the movement of the target spacecraft. Specifically, two sources of error can be identified as an error. On the one hand, the estimator depends on the precision in the image processing. On the other hand, errors in the measurement in the camera motion, $\boldsymbol{v}^{VC}$, can also produce errors in the estimation provided by Equation (11). In the next section, a target spacecraft motion estimator is proposed by using a Kalman filter.

3.3 Target spacecraft motion estimation

Different approaches can be used to filter the measurement error obtained when the image error variation due to the target motion is estimated. One of these approaches is approaches are the ones based on Kalman filters [18]. These filters, do not generate correct estimations when abrupt changes in the state vector are obtained (these abrupt changes are considered noise and the filter requires several iterations for the convergence). In this section, the formulation of a Kalman filter is presented to be applied to the specific case presented in this paper, i. e., the estimation of the motion of the target spacecraft.

In a general case, the equations of the model state and measurement can be considered as:

$$\begin{aligned} \boldsymbol{x}_{(k+1)} &= \boldsymbol{F}\boldsymbol{x}_{(k)} + \boldsymbol{v}_{(k)} \\ \boldsymbol{z}_{(k)} &= \boldsymbol{H}\boldsymbol{x}_{(k)} + \boldsymbol{w}_{(k)} \end{aligned} \tag{12}$$

where:

- $\boldsymbol{F}$ is the state transition matrix. This matrix relates the state in the previous iteration k-1 with the current state k (without noise).
- $\boldsymbol{H}$ is the measurement matrix, which relates the state with the measurement.
- It is assumed that the random variables $\boldsymbol{v}$ and $\boldsymbol{w}$ are independent. $\boldsymbol{v}$ is the noise process, and it is supposed to be with white centered noise and with covariance matrix $\boldsymbol{Q}$. $\boldsymbol{w}$ is the measurement noise. It is supposed to be with white centered noise and with covariance matrix $\boldsymbol{R}$.

The target motion components are not correlated; therefore, two independent Kalman filters are applied to each of the components $\left(\frac{\partial \widehat{e_{sx}}}{\partial t}, \frac{\partial \widehat{e_{sy}}}{\partial t}\right)$. In the next paragraphs the subscript *s* (e.g., in $\frac{\partial \widehat{e_s}}{\partial t}$) is used to represent generically any of the components, *x*, *y*. The equations of the state model and measurement of the Kalman filter are:

$$\begin{pmatrix} \left(\frac{\partial \boldsymbol{e}_s}{\partial t}\right)_{k+1} \\ \boldsymbol{\eta}_{k+1} \end{pmatrix} = \boldsymbol{F} \begin{pmatrix} \left(\frac{\partial \boldsymbol{e}_s}{\partial t}\right)_{k} \\ \boldsymbol{\eta}_{k} \end{pmatrix} + \begin{pmatrix} 0 \\ \boldsymbol{v}_{(k)} \end{pmatrix} \tag{13}$$

$$\left(\frac{\partial \widehat{\boldsymbol{e}_s}}{\partial t}\right)_{k+1} = \boldsymbol{H} \begin{pmatrix} \left(\frac{\partial \boldsymbol{e}_s}{\partial t}\right)_{k+1} \\ \boldsymbol{\eta}_{k+1} \end{pmatrix} + \boldsymbol{w}_{(k)} \tag{14}$$

where $\left(\frac{\partial \widehat{e_s}}{\partial t}\right)_k$ is the variation of the error due to the target spacecraft motion. This term needs to be measured by using equation (11). Therefore, the prediction of the state vector is given by:

$$\left(\frac{\partial \widehat{\boldsymbol{e}_s}}{\partial t}\right)_{k+1|k} = \left(\frac{\partial \widehat{\boldsymbol{e}_s}}{\partial t}\right)_{k|k} \tag{15}$$

with the matrices $\boldsymbol{F}$ and $\boldsymbol{H}$ being:

$$\boldsymbol{F} = \begin{pmatrix} 1 & 1 \\ 0 & \rho \end{pmatrix} \tag{16}$$

$$\boldsymbol{H} = \begin{pmatrix} 1 & 0 \end{pmatrix} \tag{17}$$

where ρ is the correlation grade between the successive accelerations of the target (this parameter changes between 0 and 1). In this case, the prediction and estimation equations of the Kalman filter are respectively:

$$\begin{pmatrix} \left(\frac{\partial \widehat{\boldsymbol{e}_s}}{\partial t}\right)_{k+1|k} \\ \widehat{\boldsymbol{\eta}}_{k+1|k} \end{pmatrix} = \boldsymbol{F} \begin{pmatrix} \left(\frac{\partial \widehat{\boldsymbol{e}_s}}{\partial t}\right)_{k|k} \\ \widehat{\boldsymbol{\eta}}_{k|k} \end{pmatrix} \tag{18}$$

$$\begin{pmatrix} \left(\frac{\partial \widehat{\boldsymbol{e}_s}}{\partial t}\right)_{k+1|k+1} \\ \widehat{\boldsymbol{\eta}}_{k+1|k+1} \end{pmatrix} = \begin{pmatrix} \left(\frac{\partial \widehat{\boldsymbol{e}_s}}{\partial t}\right)_{k+1|k} \\ \widehat{\boldsymbol{\eta}}_{k+1|k} \end{pmatrix} + \boldsymbol{K}_{k+1}\boldsymbol{\gamma}_{k+1} \tag{19}$$

where γ_{k+1} is the innovation between the measurement and the previous prediction. The covariance matrices of the error prediction and estimation, the gain and measure innovation are given by:

$$\begin{aligned} \boldsymbol{P}_{k+1|k} &= \boldsymbol{F}\boldsymbol{P}_{k|k}\boldsymbol{F}^T + \boldsymbol{Q} \\ \boldsymbol{P}_{k+1|k+1} &= (\boldsymbol{I} - \boldsymbol{K}_{k+1}\boldsymbol{H})\boldsymbol{P}_{k+1|k} \\ \boldsymbol{K}_{k+1} &= \boldsymbol{P}_{k+1|k}\boldsymbol{H}^T\left(\boldsymbol{H}\boldsymbol{P}_{k+1|k}\boldsymbol{H}^T + \boldsymbol{R}\right)^{-1} \\ \boldsymbol{\gamma}_{k+1} &= \left(\frac{\partial \widehat{\boldsymbol{e}_s}}{\partial t}\right)_{k+1} - \left(\frac{\partial \widehat{\boldsymbol{e}_s}}{\partial t}\right)_{k+1|k} \end{aligned} \tag{20}$$

4 On-orbit robot manipulator visual servoing

This section describes the robot manipulator dynamics and the controller designed to perform the tracking of image trajectories. First, the dynamics of the robot manipulator can be defined by the following equation:

$$\begin{bmatrix} \boldsymbol{F}_b \\ \boldsymbol{\tau} \end{bmatrix} = \begin{bmatrix} \boldsymbol{M}_{bb} & \boldsymbol{M}_{bm} \\ \boldsymbol{M}_{bm}^T & \boldsymbol{M}_{mm} \end{bmatrix} \begin{bmatrix} \ddot{\boldsymbol{x}}_b \\ \ddot{\boldsymbol{q}} \end{bmatrix} + \begin{bmatrix} \boldsymbol{c}_b \\ \boldsymbol{c}_m \end{bmatrix} \tag{21}$$

where $\ddot{\boldsymbol{q}} \in \Re^n$ is the set of accelerations of the manipulator joints, $\ddot{\boldsymbol{x}}_b = [\dot{\boldsymbol{v}}_b^T \quad \dot{\boldsymbol{\omega}}_b^T]^T \in \Re^6$ represents the linear and angular accelerations of the service spacecraft with respect the inertial coordinate frame, $\boldsymbol{M}_{bb} \in \Re^{6\times6}$ is the inertia matrix of the spacecraft, $\boldsymbol{M}_{bm} \in \Re^{6\times n}$ is the coupled inertia matrix of the spacecraft and the robot manipulator, $\boldsymbol{M}_{mm} \in \Re^{n\times n}$ is the inertia matrix of the robot manipulator; $\boldsymbol{c}_b$ and $\boldsymbol{c}_m \in \Re^6$ represents a velocity/displacement-dependent, non-linear terms for the spacecraft and robot manipulator, $\boldsymbol{F}_b \in \Re^6$ is the force and moment exerted on the service spacecraft, and $\boldsymbol{\tau} \in \Re^n$ is the applied joint torque on the manipulator. This paper assumes that no control action is applied to the base spacecraft, therefore, $\boldsymbol{F}_b = 0$. Additionally, free-floating conditions are considered: the base spacecraft moves when the manipulator performs a motion. With these considerations Equation (21) can be written as:

$$\boldsymbol{M}_{mm}^*\ddot{\boldsymbol{q}} + \boldsymbol{H}^* = \boldsymbol{\tau} \tag{22}$$

where $\boldsymbol{M}_{mm}^* \in \Re^{n\times n}$ represents the generalized inertia matrix of the manipulator and service spacecraft and $\boldsymbol{H}^* \in \Re^n$ represents the generalized Coriolis and centrifugal matrix:

$$\boldsymbol{M}^{*}_{mm} = \boldsymbol{M}_{mm} - \boldsymbol{M}^{T}_{bm}\boldsymbol{M}^{-1}_{bb}\boldsymbol{M}_{bm} \tag{23}$$

$$\boldsymbol{H}^{*} = \boldsymbol{c}_{m} - \boldsymbol{M}^{T}_{bm}\boldsymbol{M}^{-1}_{bb}\boldsymbol{c}_{b} \tag{24}$$

Additionally, the linear and angular momenta of the robot manipulator and base spacecraft $\left(\boldsymbol{\ell}^{\mathrm{T}}, \boldsymbol{\Psi}^{\mathrm{T}}\right)^{\mathrm{T}} \in \Re^{6}$ are:

$$\begin{bmatrix}\boldsymbol{\ell}\\ \boldsymbol{\Psi}\end{bmatrix} = \boldsymbol{M}_{bb}\dot{\boldsymbol{x}}_{b} + \boldsymbol{M}_{bm}\dot{\boldsymbol{q}} \tag{25}$$

where $\dot{\boldsymbol{q}} \in \Re^{\mathrm{n}}$ are the manipulators' joint velocities, and $\dot{\boldsymbol{x}}_{b} = [\boldsymbol{v}_{b}^{T} \quad \boldsymbol{\omega}_{b}^{T}]^{T} \in \Re^{6}$ represents the linear and angular velocities of the service spacecraft in the inertial coordinate frame. The relationship between the time derivatives of the joint positions, $\dot{\boldsymbol{q}}$, and the corresponding end-effector's absolute linear and angular velocities can be obtained by the manipulator Jacobian, $\boldsymbol{J}_{\mathrm{m}} \in \Re^{6\times \mathrm{n}}$, and the Jacobian matrix of the service spacecraft, using the following relationship:

$$\dot{\boldsymbol{x}}_{e} = \boldsymbol{J}_{m}\dot{\boldsymbol{q}} + \boldsymbol{J}_{b}\dot{\boldsymbol{x}}_{b} \tag{26}$$

To obtain the equation that relates joint velocities and the velocities of the manipulator end effector we can combine Equations (26) and (25), obtaining the following equation:

$$\dot{\boldsymbol{x}}_{e} = \boldsymbol{J}_{g}\dot{\boldsymbol{q}} + \dot{\boldsymbol{x}}_{ge} \tag{27}$$

where:

$$\boldsymbol{J}_{g} = \boldsymbol{J}_{m} - \boldsymbol{J}_{b}\boldsymbol{M}^{-1}_{bb}\boldsymbol{M}_{bm} \tag{28}$$

$$\dot{\boldsymbol{x}}_{ge} = \boldsymbol{J}_{b}\boldsymbol{M}^{-1}_{bb}\begin{bmatrix}\boldsymbol{\ell}\\ \boldsymbol{\Psi}\end{bmatrix} \tag{29}$$

In Equation (27), $\boldsymbol{J}_{g}$ is the Generalized Jacobian Matrix which relates the joint velocities of the manipulator arm and the end effector velocities. Additionally, $\dot{\boldsymbol{x}}_{\mathrm{ge}}$, is an offset velocity due to the non-zero momentum.

The previous differential kinematics is required to be extended to determine the relationship between image and joint coordinates. As previously indicated, the interaction matrix, $\boldsymbol{L}_{s}$, relates the velocities of the extracted visual features in the image space, $\dot{\boldsymbol{s}}$, and the end effector motion, $\dot{\boldsymbol{x}}_{e}$. Taking into account this last relationship, Equation (27) can be expressed as:

$$\dot{\boldsymbol{s}} = \boldsymbol{L}_{s}\boldsymbol{J}_{g}\dot{\boldsymbol{q}} + \boldsymbol{L}_{s}\dot{\boldsymbol{x}}_{ge} = \boldsymbol{L}_{J}\dot{\boldsymbol{q}} + \dot{\boldsymbol{s}}_{ge} \tag{30}$$

where $\boldsymbol{L}_{J}$ is the product of the interaction matrix and the robot Jacobian. This matrix relates joint velocities and the time derivative of the extracted visual features. Additionally, $\dot{\boldsymbol{s}}_{\mathrm{ge}}$ is the projection in the image space of the velocity $\dot{\boldsymbol{x}}_{\mathrm{ge}}$. Therefore, the control action given in Equation (7) can be extended taking into account the free-floating conditions and the estimation of the motion of the target spacecraft using the following equation:

$$\dot{\boldsymbol{q}} = -\lambda_3 \boldsymbol{L}_J^{+} \left(\boldsymbol{e}_s - \frac{\partial \widehat{\boldsymbol{e}_s}}{\partial t} - \dot{\boldsymbol{s}}_{ge} \right) \tag{31}$$

5 Results

This section presents the main results obtained in the application of the proposed controller to perform the manipulator guidance considering the on-orbit servicing scenario detailed in Section 2. The initial position of the target spacecraft is (0,10, 0) m with respect to the base spacecraft coordinate frame. The base spacecraft is left free to move in a free-floating condition when the robotic arms operate. No external forces are applied to the base spacecraft. Two different kinds of maneuvres are presented in this paper. In the first one, the robotic manipulator uses visual information extracted from the target spacecraft to perform a motion in only single direction (x or z with respect the T coordinate frame), maintaining the distance with respect to the target spacecraft. The second experiments use visual information to perform more complex motions which require displacements in several directions.

5.1 Visual controller to guide the manipulator in a single movement

In this case, the visual information obtained by the robotic camera is used to guide the robotic manipulator in just one direction. As previously indicated, the visual information to be fed to the controller is based on the recognition and tracking of four visual feature points extracted from the target spacecraft. The coordinates of the initial features extracted by the camera in both the maneuvres under analysis are $\boldsymbol{s}_i = \begin{bmatrix} \boldsymbol{s}_{ix} \\ \boldsymbol{s}_{iy} \end{bmatrix}^T = \begin{bmatrix} 452 & 556 & 572 & 468 \\ 556 & 572 & 468 & 452 \end{bmatrix}^T$. To obtain a displacement along y-direction the desired features to be included in Equation (31) are the following ones:

$$\boldsymbol{s}_d = \begin{bmatrix} \boldsymbol{s}_{dx} \\ \boldsymbol{s}_{dy} \end{bmatrix}^T = \begin{bmatrix} 452 & 556 & 572 & 468 \\ 631 & 648 & 543 & 527 \end{bmatrix}^T \tag{32}$$

Analogously, to obtain a displacement along z-direction, the following features will be considered as the desired ones:

$$\boldsymbol{s}_d = \begin{bmatrix} \boldsymbol{s}_{dx} \\ \boldsymbol{s}_{dy} \end{bmatrix}^T = \begin{bmatrix} 529 & 633 & 649 & 545 \\ 556 & 572 & 468 & 452 \end{bmatrix}^T \tag{33}$$

The results obtained in the application of the controller using both sets of desired visual features are indicated in Fig. 2. Fig. 2.a, and Fig. 2.d represents the image trajectory of the four visual features. From the analysis of such figures, the visual features describe straight trajectories from the initial to the desired features. In both cases, the desired visual features are achieved. However, in order to show more clearly the motion performed by the servicing spacecraft, the 3D trajectories described by the robot manipulator are shown in Fig. 2.b, and Fig. 2.e, respectively. The trajectory described by the robotic manipulator is in blue in both figures. The manipulator end-effector correctly performed displacements along y and z directions, maintaining a

constant distance with respect to the target spacecraft. Finally, Fig. 2.c, and Fig. 2.f represents the manipulator joint torques and the force and moments applied to the base spacecraft due to the motion of the manipulator.

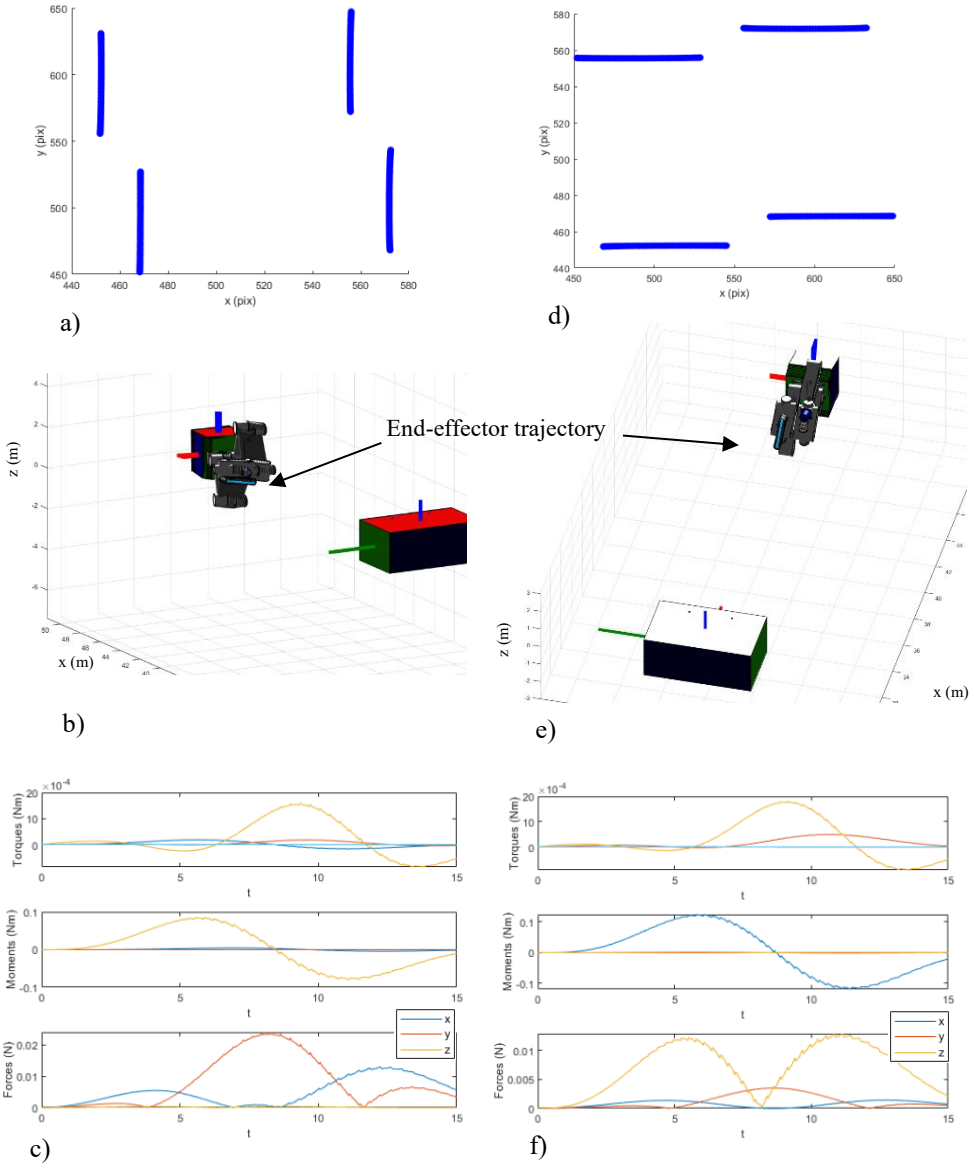

Fig. 2. a) image trajectory of the extracted visual features (displacement in y-direction). b) 2d trajectory of the servicing spacecraft (displacement in y-direction). c) Joint applied torques, and force and moments in the base spacecraft (displacement in y-direction). d) image trajectory of the extracted visual features (displacement in z-direction). e) 2d trajectory of the servicing spacecraft (displacement in z-direction). f) Joint applied torques, and force and moments in the base spacecraft (displacement in z-direction).

5.2 Visual controller to guide the manipulator following complex motion directions

The second simulation assesses the applicability of the proposed strategy when the desired motion implies a simultaneous displacement in several directions. As previously indicated, the visual information extracted from the target spacecraft is based on the four visual feature points of the target seen and extracted from the images captured by the camera. The coordinates of the initial features extracted by the camera are the same indicated in the experiments in Section 5.1, while the desired features to be included in Equation (31) are the following:

$$\boldsymbol{s}_d = \begin{bmatrix} \boldsymbol{s}_{dx} \\ \boldsymbol{s}_{dy} \end{bmatrix}^T = \begin{bmatrix} 374 & 478 & 494 & 390 \\ 480 & 496 & 392 & 375 \end{bmatrix}^T \tag{34}$$

By considering these last visual features, a movement of the end effector is obtained along both y- and z-directions simultaneously while keeping fixed the distance of the base of the spacecraft and the target spacecraft. Additionally, another case can be considered by setting as desired visual features the following ones:

$$\boldsymbol{s}_d = \begin{bmatrix} \boldsymbol{s}_{dx} \\ \boldsymbol{s}_{dy} \end{bmatrix}^T = \begin{bmatrix} 546 & 656 & 673 & 563 \\ 594 & 613 & 500 & 486 \end{bmatrix}^T \tag{35}$$

If these last visual features are used, the manipulator robot performs an approach to the target spacecraft with a displacement along both y- and z- directions simultaneously. The results obtained in the application of the controller using both sets of desired visual features are indicated in Fig. 3 and Fig. 4. The 3D trajectories described by the robot manipulator in both experiments are represented in Fig. 3. Fig. 4.a, and Fig. 4.c represents the image trajectory of the four visual features in the image plane. The visual features describe a straight right trajectory from the initial and the desired features but, differently from Fig. 2.a, and Fig. 2.d, their trajectories move along the diagonal of the image plane. In both cases, the desired visual features are achieved. As shown in Fig. 3.a, the manipulator performs a displacement in a plane parallel to the target spacecraft, maintaining a fixed distance with respect to the target. As it is shown in Fig. 3.b, in this last trajectory the manipulator robot also performs an approach to the target, achieving the desired pose. Finally, Fig. 4.b, and Fig. 4.d represents the manipulator joint torques, and the force and moments applied to the base spacecraft due to the motion of the manipulator.

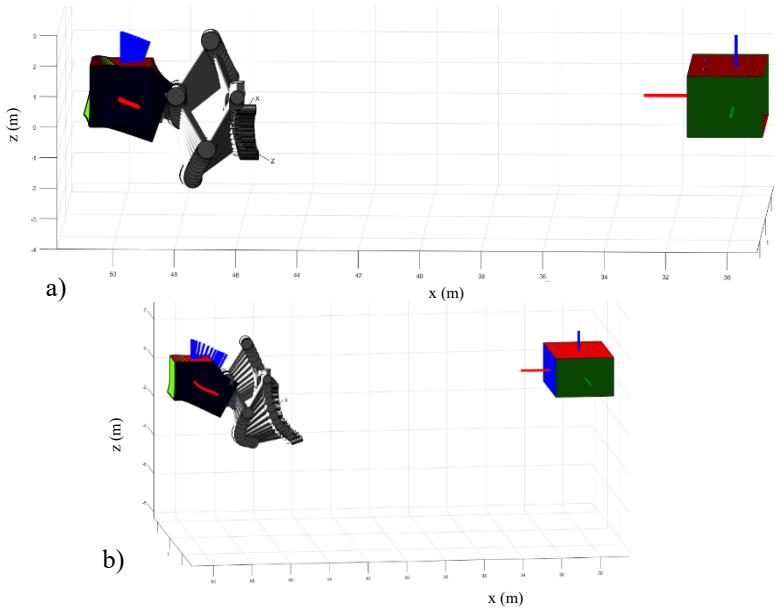

Fig. 3. a) 3D trajectory of the servicing spacecraft (trajectory 1). b) 3D trajectory of the servicing spacecraft (trajectory 2).

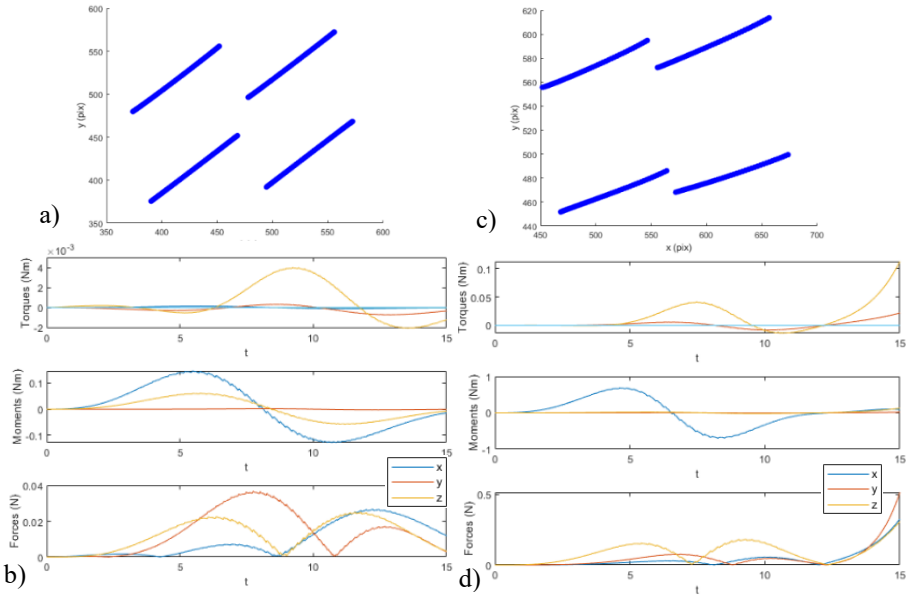

Fig. 4. a) image trajectory of the extracted visual features (trajectory 1). b) Joint applied torques, and force and moments in the base spacecraft (trajectory 1). c) image trajectory of the extracted visual features (trajectory 2). d) Joint applied torques, and force and moments in the base spacecraft (trajectory 2).

6 Conclusions

The paper presented a visual servoing algorithm suitable for on-orbit servicing and manipulation. The algorithm is applicable to a spacecraft equipped with two-arm manipulator. The two arms are dedicated to manipulation and observation tasks, respectively.

A visual servoing controller independent from the observed scene's point of view was consequently developed. The virtual features could be virtually reconstructed following a specific pattern seen on the target body and consequently assumed attached to the end effector of the operating manipulator. A Kalman filter was implemented to estimate the movements of the visual features due to the target satellite motion as well as these due to the intrinsic movement of the service spacecraft due to the manipulator operations.

Numerical results show that the so-developed controller was able to drive the manipulator in such a way to make the virtual features match the real features on the target body even when the target was relatively moving with respect to the base of the sercicing spacecraft.

Further studies will assess the robustness of the proposed controller against environmental torques and forces, evaluate the performance of the controller with different frame rates of the camera, and compare the results with other tracking controllers.

References

1. Froehlich, A., On-Orbit Servicing: Next Generation of Space Activities. Springer, Cham (2020). https://doi.org/10.1007/978-3-030-51559-1
2. UNITED NATIONS Office for Outer Space Affairs, https://www.unoosa.org/oosa/osoindex, last accessed 2022/02/18.
3. Liu, Y., Zhao, Y., Tan, C., Liu, H., Liu, Y., Economic value analysis of on-orbit servicing for geosynchronous communication satellites, Acta Astronautica, Vol. 180, 2021, pp. 176-188, https://doi.org/10.1016/j.actaastro.2020.11.040.
4. Flores-Abad A., Ma O., Pham K., Ulrich S. A review of space robotics technologies for on-orbit servicing. Prog. Aerosp. Sci., 68 (2014), 1-26. https://doi.org/10.1016/j.paerosci.2014.03.002
5. Moghaddam, B. M., Chhabra, R., On the guidance, navigation and control of in-orbit space robotic missions: A survey and prospective vision, Acta Astronautica, 184 (2021), 70-100, https://doi.org/10.1016/j.actaastro.2021.03.029.
6. Felicetti, L., Gasbarri, P., Pisculli, A., Sabatini, M., Palmerini, G.B., Design of robotic manipulators for orbit removal of spent launchers' stages, Acta Astronautica, 119 (2016), 118-130, doi: 10.1016/j.actaastro.2015.11.012.
7. Ramón, J.L., Pomares, J., Felicetti, L., Direct visual servoing and interaction control for a two-arms on-orbit servicing spacecraft, Acta Astronautica, Vol. 192, 2022, pp. 368-378, https://doi.org/10.1016/j.actaastro.2021.12.045.
8. Cassinis, L.P., Fonod, R., Eberhard Gill, Review of the robustness and applicability of monocular pose estimation systems for relative navigation with an uncooperative spacecraft, Progress in Aerospace Sciences, 110 (2019), https://doi.org/10.1016/j.paerosci.2019.05.008.

9. Peng, J., Xu, W., Liu, T., Yuan, H., Liang, B., End-effector pose and arm-shape synchronous planning methods of a hyper-redundant manipulator for spacecraft repairing, Mechanism and Machine Theory, 155 (2021) https://doi.org/10.1016/j.mechmachtheory.2020.104062.
10. Wang, H., Guo, D., Xu, H., Chen, W., Liu, T., Leang, K. K., Eye-in-Hand Tracking Control of a Free-Floating Space Manipulator, IEEE Transactions on Aerospace and Electronic Systems, 53(4) (2017) 1855-1865, https://doi.org/10.1109/TAES.2017.2674218.
11. Ramon, J.; Pomares, J. and Felicetti, L. (2021). On-orbit Free-floating Manipulation using a Two-arm Robotic System. In Proceedings of the 2nd International Conference on Robotics, Computer Vision and Intelligent Systems - ROBOVIS, pages 57-63. DOI: 10.5220/0010712100003061
12. Xu, R., Luo, J., Wang, M., Kinematic and dynamic manipulability analysis for free-floating space robots with closed chain constraints, Robotics and Autonomous Systems, 130 (2020), doi: 10.1016/j.robot.2020.103548.
13. Ramón, J.L., Pomares, J., Felicetti, L., Direct visual servoing and interaction control for a two-arms on-orbit servicing spacecraft, Acta Astronautica, Vol. 192, 2022, pp. 368-378, https://doi.org/10.1016/j.actaastro.2021.12.045.
14. Ma, G., Jiang, Z., Li, H., Gao, J., Yu, Z., Chen, X., Hand-eye servo and impedance control for manipulator arm to capture target satellite safely, Robotica, 33 (2015) 848–864. https://doi.org/10.1017/S0263574714000587.
15. Chaumette, F.; Hutchinson, S. Visual servo control. I. Basic approaches, IEEE Robotics & Automation Magazine, 2006, 13(4), 82-90.
16. Alepuz, J.P., Emami, M.R., Pomares, J., Direct image-based visual servoing of free-floating space manipulators. Aerospace Science and Technology 55 (2016), 1-9, https://doi.org/10.1016/j.ast.2016.05.012
17. Pomares, J., Felicetti, L., Pérez, J., Emami, M.R., Concurrent image-based visual servoing with adaptive zooming for non-cooperative rendezvous maneuvers. Advances in Space Research, 61(3), (2018), 862-878, https://doi.org/10.1016/j.asr.2017.10.054.
18. Salehian, M., RayatDoost S., Taghirad, H. D. Robust unscented Kalman filter for visual servoing system, The 2nd International Conference on Control, Instrumentation and Automation, (2011), 1006-1011, https://doi.org/10.1109/ICCIAutom.2011.6356799.

Cranfield University

CERES https://dspace.lib.cranfield.ac.uk

School of Aerospace, Transport and Manufacturing (SATM) Staff publications (SATM)

2022-11-10

Visual guidance of an on-orbit free-floating manipulator using a mobile camera

Ramón, José Luis

Springer

Ramón JL, Pomares J, Felicetti L. (2022) Visual guidance of an on-orbit free-floating manipulator using a mobile camera. In: Galambos, P., Kayacan, E., Madani, K. (eds), ROBOVIS 2021, Communications in Computer and Information Science, Springer, Volume 1667, pp. 114-130 https://doi.org/10.1007/978-3-031-19650-8_6

Downloaded from Cranfield Library Services E-Repository